Journal of the Korean Physical Society, Vol. 65, No. 11, December 2014, pp. 1873∼1882

Planar Sheath Model in Dusty Plasmas with a Two-temperature Electron Distribution

T. H. Chung*
Department of Physics, Dong-A University, Busan 604-714, Korea

(Received 17 July 2014, in final form 12 September 2014)

The two-temperature electron distribution is found to affect significantly the dust grain surface potential or the dust grain charge. Based on the Sagdeev potential approach, a modified sheath criterion including the effect of a two-temperature electron distribution is established theoretically. A one-dimensional fluid model is utilized to describe the sheath at a plasma-wall boundary in dusty plasmas with a two-temperature electron distribution. The effects of the population ratio of hot to cold electrons and of the temperature ratio of hot to cold electrons on the characteristics of the dusty plasma-plane wall (or probe) boundary are investigated. The spatial distributions of the electric potential and of the velocities and densities of the plasma species including those of dust grains, the electric force, and the ion drag force are calculated. With increasing population ratio of hot to cold electrons, the sheath width broadens, and the ion flux to the wall increases whereas the ion drift velocity decreases. An enhanced temperature ratio of hot to cold electrons causes the sheath width to broaden and the ion flux to the wall to increase.

PACS numbers: 52.35.Ra, 52.25.-b, 52.25.Vy, 52.80.Pi
Keywords: Dusty plasma, Two-temperature electron distribution, Plane sheath, Fluid model
DOI: 10.3938/jkps.65.1873

I. INTRODUCTION

There has been a great deal of interest in understanding dusty plasmas not only because of the ubiquity of such plasmas in space [1–3] but also because of their vital role in devices for plasma-assisted material processing [4,5] and in fusion devices [6,7]. In plasma processing reactors, because dust particles appear as contamination to etching, sputtering, and deposition processes, dust is an unwanted element and attention has been drawn to finding techniques for removing it [8–10].

The main observations of dust in glow discharges have been distinct cloud formations at the plasma-sheath boundary near the rf-powered electrode [11–13]. The plasma sheath provides fluxes of ions, radicals, and dust particles to the substrate. Some important issues in dusty plasmas include the problem of determining the charge and the density of dust particles, the sheath structure, and the spatial distribution of the plasma species [14–26]. The dust particles can significantly influence the sheath properties due to their continuous selective collection of background electrons and ions, which can cause an essential change in both the electron and the ion energy distribution functions as well as an ion flux in the sheaths. As a result, the spatial distributions of plasma parameters in the sheaths can be significantly changed, including the potential profile, which determine the properties of the dust oscillations and the waves in sheaths [27].

Plasmas with two-temperature electron distributions are rather frequently encountered. For example, tokamak edge plasmas often have high energy tails [28], strong electron-beam-plasma interactions can result in such electron distributions, and very often, simple hot-cathode discharge plasmas also have two-temperature electron distributions [29]. Two-temperature Maxwellian electron distributions may also occur in low-temperature plasmas due to inelastic electron collisions with excited atoms, ions and molecules as well as in the expanding corona of a plasma heated by a laser and in negative-ion sources [27]. Because hot electrons are continuously generated, non-equilibrium nature persists between hot and cold electrons. Understanding the effect of the two populations of electrons on the plasma sheath has been of significant importance because the plasma sheath determines the plasma-wall interactions and strongly affects the edge plasma properties [30].

In a previous paper [31], a fluid model was developed for studying the structure of the plasma - planar wall boundary in low-pressure dusty plasmas. In this study, the model is extended to include the effect of the two-temperature electron distribution on the characteristics of the dusty plasma-plane wall (or probe) boundary. The spatial distributions of the electric potential

*E-mail: thchung@dau.ac.kr

and of the velocities and the densities of charged species (ions, electrons, and dust grains) are calculated in front of a negatively-biased planar wall (or probe) immersed in dust-containing plasmas with two-temperature electron distributions. Also, the evolutions of the dust charge number, electric force, and ion drag force in the cathode sheath are calculated for a wide range of control parameters. Especially, the effects of the two-temperature electron distribution (the hot electron population and the temperature ratio of hot to cold electrons) on the ion flux collected by the probe are investigated.

This paper is organized as follows: In Sec. II, the surface potential of a dust grain immersed in a plasma with a two-temperature electron distribution is calculated, and its variation with the Havnes parameter is given. To investigate the effect of the two-temperature electron distribution, we introduce the electrostatic sheath model, the basic fluid equations and assumptions, and the numerical method. Section III describes a simplified model that provides a modified Bohm criterion indicating the velocities of the ions entering the sheath. Section IV gives the results of numerical simulations for the sheath structure. The spatial distributions of the densities and the velocities of the plasma species and the dust particles are presented, and the effects of the two-temperature electron distribution on those parameters are discussed. Finally, the paper is concluded in Sec. V with a summary of the main results and a brief discussion.

II. MODEL EQUATIONS

We consider a plasma with a two-temperature electron distribution consisting of cold and hot electrons (temperatures T_L and T_H) and singly-charged positive ions (temperature T_i). When the dust particles (density n_d, grain radius a) are immersed in the plasma, they typically acquire a high negative charge (up to a few thousand electrons) due to the high electron mobility, which modifies the equilibrium charge quasineutrality condition to [10]

$$n_i - n_{eL} - n_{eH} - Z_d n_d = 0, \tag{1}$$

where n_i, n_{eL}, and n_{eH} are the densities of ions, and cold and hot electrons, respectively, and Z_d is the dust charge number. In this study, the dominant charging mechanism is assumed to be the accumulation of electrons and ions at the surface of the dust grain. Dust particles are assumed to be spherical. Because ions are heavier than electrons, the ion current to a dust particle is smaller than the electron current, and the dust particle becomes negatively charged. In laboratory plasmas where secondary emission processes due to radiation absorption and to hot particle impacts are small, the dust particle's net charge is negative [26]. The thermal currents of cold and hot electrons flowing onto the dust particle's surface are given by

$$I_{ej} = -\pi a^2 n_{ej} e \left(\frac{8kT_j}{\pi m_e}\right)^{1/2} \exp(\frac{e\phi_d}{kT_j}) \quad (\phi_d < 0), \tag{2}$$

$$I_{ej} = -\pi a^2 n_{ej} e \left(\frac{8kT_j}{\pi m_e}\right)^{1/2} \left(1 + \frac{e\phi_d}{kT_j}\right) \quad (\phi_d > 0), \tag{3}$$

where $j = L$ (cold electron) and H (hot electrons), e is the electron charge, k is the Boltzmann constant, m_e is the mass of an electron, and ϕ_d is the surface floating potential of the dust particle ($\phi_d = -Z_d e/4\pi\varepsilon_0 a$). The orbit motion limited (OML) theory can be used to calculate the charging ion currents as

$$I_i = \pi a^2 n_i e \left(\frac{8kT_i}{\pi m_i}\right)^{1/2} \left(1 - \frac{e\phi_d}{kT_i}\right) \quad (\phi_d < 0), \tag{4}$$

where m_i is the mass of an ion. For positively-charged dust grains ($\phi_d > 0$), I_i has a dependence of $\exp(-e\phi_d/kT_i)$ instead of $1 - e\phi_d/kT_i$.

Requiring a zero net current onto the negatively charged dust particle, Eqs. (2) and (4), and using the charge neutrality condition, Eq. (1), we have

$$\frac{n_{eL}}{n_i}\sqrt{\frac{m_i T_L}{m_e T_i}} \exp\left(\frac{e\phi_d}{kT_L}\right) + \frac{n_{eH}}{n_i}\sqrt{\frac{m_i T_H}{m_e T_i}} \exp\left(\frac{e\phi_d}{kT_H}\right) + \frac{e\phi_d}{kT_i} - 1 = 0. \tag{5}$$

If we introduce the Havnes parameter $P = (4\pi\varepsilon_0 akT_L/e^2)(n_d/n_0)$, the reduced surface floating potential $\tilde{\phi}_d = Z_d e^2/4\pi\varepsilon_0 akT_L$ (ε_0 is the permittivity of the vacuum), and $\delta^2 = n_i/n_{eL}$, and if we assume that the ion density is unaffected by the presence of the dust component and thus $n_i = const = n_0$, we have

$$\frac{n_{eH}}{n_i} = 1 - \frac{1}{\delta^2} - P\tilde{\phi}_d. \tag{6}$$

Then, Eq. (5) gives the following equation for $\tilde{\phi}_d$

$$\sqrt{\frac{m_i}{m_e}}\gamma\left[\frac{1}{\delta^2}\exp(-\tilde{\phi}_d) + \sqrt{\beta}\,(1 - \frac{1}{\delta^2} - P\tilde{\phi}_d) \times \exp(-\tilde{\phi}_d/\beta)\right] = 1 + \gamma\tilde{\phi}_d, \tag{7}$$

where β and γ define the temperature ratios $\beta = \frac{T_H}{T_L}$ and $\gamma = \frac{T_L}{T_i}$.

Therefore, for a given $P_0 = (4\pi\varepsilon_0 akT_L/e^2)(n_{d0}/n_0)$, Eq. (7) provides the dust charge (via $\tilde{\phi}_{d0}$) at the plasma bulk region. The charging time is inversely proportional to the plasma density and the dust grain radius and is proportional to the square root of the ion temperature. Numerically, the charging time is on the order of tens of microseconds in the operating region considered in the paper. Although it varies depending on the parameters, the order of the charging time is not changed much and

is much shorter than the measurement time. Fluid theory is valid on time scales larger than charging time. It can also be valid for slightly slower phenomena such as ELMs in fusion devices. In this paper, the grain charge was treated as a continuous variable. Because the electron and the ion fluxes in reality represent sequences of events bound to electron and ion absorption by the grain surface, the grain charge fluctuates around its average value and may cause instabilities in the grain's oscillation [32]. Here, we neglect grain charge fluctuations and consider an electrostatic plasma sheath in steady state.

In order to obtain some physical insight into the theoretical analysis, we introduce a set of reference parameters that are typical for plasma processing experiments. The plasma parameters are chosen to be $n_0 = 1.5 \times 10^{10} cm^{-3}$, $T_L = 2$ eV, $T_i = 0.04$ eV, and the average particle size $a = 6$ μm. We fix the plasma density n_0, but keep the Havnes parameter P_0 as a free quantity, varying it in a physically-meaningful range of dust densities.

Figure 1(a) shows the the calculated evolution of $\tilde{\phi}_{d0}$ with P_0 for different δ^2 (= 1.1, 1.2, and 1.4) in Ar plasmas. As n_{d0} is increased, the intergrain spacing decreases, and the average grain charge is reduced. The evolution of $\tilde{\phi}_{d0}$ with P_0 has a sensitive dependence on δ^2. A larger δ^2 indicates a larger population of hot electrons. An increase in δ^2 leads to an increase in the dust grain's surface potential. This is attributable to the increased electron current flowing onto the dust particle's surface. Figure 1(b) illustrates how the behavior of the $\tilde{\phi}_{d0}$ vs P_0 curves are modified by the temperature ratio of hot to cold electrons (β (= 5, 10, and 20)). In the relatively low P_0 region, a larger β results in an increase in the reduced surface potential. However, as P_0 is increased (n_{d0} is increased), the dependence of $\tilde{\phi}_{d0}$ on both δ^2 and β becomes weak. This can be explained by the fact that many background electrons have already been attached to the dust particle in the higher P_0 region.

We assume that the sheath region lies between z=0 and the wall (the presheath is neglected) with the plasma filling the half space $z < 0$, where z is the position along the vertical axis, which is in the same direction as gravity [24]. The plasma variables are calculated along the distance from the plasma region to any arbitrary small distance near the planar wall by using a set of coupled equations including the steady-state fluid equations of continuity and motion for the ion and the dust particle, and Poisson's equation with a Boltzmann electron [33, 34]. The model equations are developed for a planar geometry with the assumption of one-dimensional motion of charged species towards the wall.

The ions are governed by the continuity and momentum balance equations

$$\frac{d}{dz}(n_i v_i) = \nu_{iz} n_e, \tag{8}$$

$$m_i n_i v_i \frac{dv_i}{dz} = -e n_i \frac{d\phi}{dz} - \frac{dp_i}{dz} - m_i(n_{eL} + n_{eH})\nu_{iz} v_i - m_i n_i(\nu_{in} + \nu_{id}) v_i, \tag{9}$$

where p_i and v_i are the pressure and the fluid velocity of the ions, ν_{iz} is the ionization frequency, ν_{in} and ν_{id} are the ion momentum-transfer collision frequencies with neutrals and with dust particles, respectively, and ϕ is the electric potential. The third term on the right-hand side of Eq. (9) represents the decrease in the fluid momentum as ions are born at rest [35]. The fourth term represents ion drag forces due to collisions with neutrals and dust particles [24]. The ν_{in} and the ν_{id} can be written as [10]

$$\nu_{in} = n_n \sigma_{in} \sqrt{\frac{T_i}{m_i}},\ \nu_{id} = n_d \sigma_{eff} \sqrt{\frac{T_i}{m_i}}, \tag{10}$$

where n_n is the neutral number density, and σ_{in} and σ_{eff} are the momentum transfer cross-sections for ion-neutral collisions and for ion-dust collisions, respectively. The effective scattering cross-section for ion-dust collisions can be written as

$$\frac{1}{\sigma_{eff}} = \frac{1}{\sigma_{id}} + \frac{4}{\pi \triangle^2}, \tag{11}$$

where $\sigma_{id} = (2\sqrt{2\pi}/3)(\tilde{\phi}_d \gamma a)^2 \Lambda$ (Λ being the modified Coulomb logarithm [10,36]) is the scattering cross-section for an individual grain and the second term represents a cross section corresponding to the largest admissible impact parameter $\sim \triangle/2$ ($\triangle \simeq n_{d0}^{-1/3}$ is the average interparticle distance). The σ_{eff} decreases with increasing P_0. In very diluted dust formations ($P \to 0$), the σ_{eff} mainly consists of the scattering cross-section for an individual isolated grain while in extremely dense clouds ($P \to \infty$), the $\sigma_{eff} \to \pi\triangle^2/4$ [10]. As γ is decreased (*i.e.*, T_i is increased for a fixed T_L), the cross-section becomes lower due to the higher thermal motion of ions. We should note that ν_{id} depends strongly on n_d, a (thus, P_0), and γ.

Poisson's equation is written as

$$\varepsilon_0 \frac{d^2\phi}{dz^2} = -e\,(n_i - n_{eL} - n_{eH}) + e Z_d n_d. \tag{12}$$

We assume that cold and hot electrons follow Boltzmann energy distributions:

$$n_{eL} = n_{eL0} \exp\left(\frac{e\phi}{kT_L}\right),\ n_{eH} = n_{eH0} \exp\left(\frac{e\phi}{kT_H}\right), \tag{13}$$

where n_{eL0} and n_{eH0} are the cold and the hot electron densities at the plasma bulk region. .

Among the forces acting on the dust particles, the electric, gravitational, and ion drag forces are considered. The particulate trapping is clearly caused by the force balance between the electrostatic potential and the gravity, as well as by the ion drag due to ions streaming to

the electrode. Therefore, the equation of motion for a dust particle is written as

$$m_d v_d \frac{dv_d}{dz} = eZ_d \frac{d\phi}{dz} + F_g + F_i, \tag{14}$$

where v_d is the velocity of the dust particle, $F_g (= 4\pi a^3 \rho_d g/3)$ is the gravitational force, and F_i is the ion drag force, which is given for superthermal ions by [19, 36]

$$F_i = \pi a^2 n_i m_i v_i^2 \left(1 - \frac{2e\phi_d}{m_i v_i^2}\right) + \frac{4\pi a^2 n_i (e\phi_d)^2 \bar{\Lambda}}{m_i v_i^2}, \tag{15}$$

with $\bar{\Lambda}$ being the Coulomb logarithm given by

$$\bar{\Lambda} = \ln\left[\frac{\frac{-e\phi_d a}{m_i v_i^2} + \lambda_D}{\frac{-e\phi_d a}{m_i v_i^2} + a}\right]. \tag{16}$$

The charge number of a micron-size dust particle (Z_d) in the sheath can be determined by the electron and the ion currents striking the particle.

We assume that the dust particle flux is conserved in the sheath as

$$\frac{d}{dz}(n_d v_d) = 0. \tag{17}$$

The variations of the plasma variables in the plasma-wall transition region can be characterized with the electron Debye length because the sheath width extends only a few electron Debye lengths. The solution to the model equations describes the structure of the sheath region in front of a planar wall. We have the following dimensionless functions and parameters:

$$\begin{aligned} &\xi = \frac{z}{\lambda_D}, \tilde{n} = \frac{n_i}{n_{i0}}, \tilde{n}_L = \frac{n_{eL}}{n_{eL0}}, \tilde{n}_H = \frac{n_{eH}}{n_{eH0}}, \\ &\tilde{n}_d = \frac{n_d}{n_{eL0}}, u = \frac{v_i}{c_s}, u_d = \frac{v_d}{c_{sd}}, \eta = -\frac{e\phi}{kT_L}, \\ &q = \frac{\lambda_D \nu_{iz}}{c_s}, \delta_{in} = \frac{\nu_{in}}{\nu_{iz}}, \delta_{id} = \frac{\nu_{id}}{\nu_{iz}}, \end{aligned} \tag{18}$$

where c_s is the ion acoustic speed ($=\sqrt{kT_L/m_i}$), c_{sd} is the dust acoustic speed ($=\sqrt{ZkT_L/m_d}$) ($Z = P_0/(1 - P_0\tilde{\phi}_{d0})\tilde{n}_{d0}$) [23,24], and λ_D is the cold electron's Debye length. The q, sometimes called the non-neutrality parameter, is a measure of the ionization rate.

The dimensionless equations of ion continuity and momentum balance for the ion and the dust particle, and Poisson's equation are written as follows:

$$\delta^2 \frac{d}{d\xi}(\tilde{n}u) = q\left[e^{-\eta} + (\delta^2 - 1 - \delta^2\tilde{\phi}_d P_0)e^{-\eta/\beta}\right], \tag{19}$$

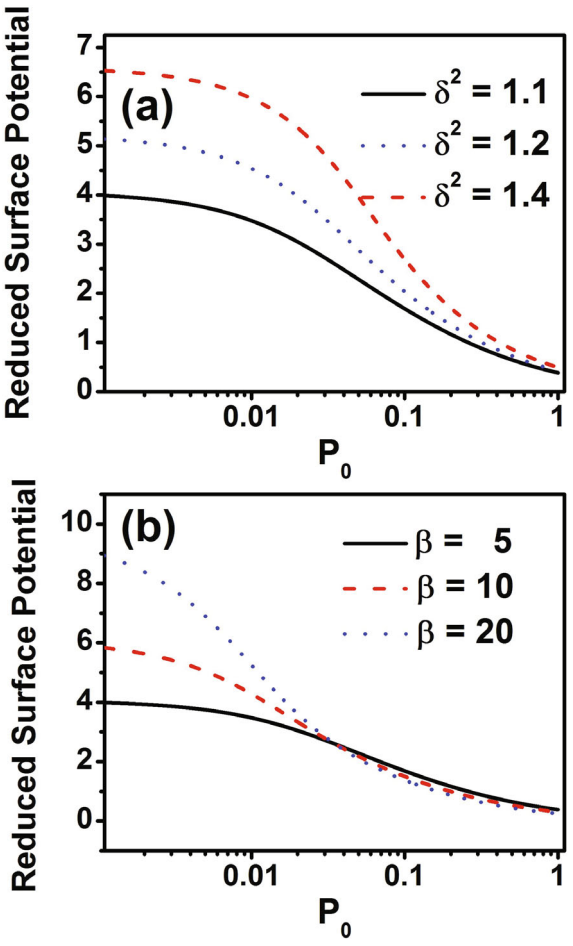

Fig. 1. (Color online) (a) Calculation of the reduced surface potential ($\tilde{\phi}_{d0}$) as a function of P_0 based on hot ion theory for different δ^2 (= 1.1, 1.2, 1.4). (b) Calculation of the reduced surface potential ($\tilde{\phi}_{d0}$) as a function of P_0 based on cold ion theory for different β (= 5, 10, 20).

$$\begin{aligned} &\left(u - \frac{1}{\gamma u}\right)\frac{du}{d\xi} \\ &= \frac{d\eta}{d\xi} - \frac{qu\left[e^{-\eta} + (\delta^2 - 1 - \delta^2\tilde{\phi}_d P_0)e^{-\eta/\beta}\right]}{\delta^2\tilde{n}} \\ &- \frac{q\left[e^{-\eta} + (\delta^2 - 1 - \delta^2\tilde{\phi}_d P_0)e^{-\eta/\beta}\right]}{\delta^2\gamma\tilde{n}u} - q(\delta_{in} + \delta_{id})u, \end{aligned} \tag{20}$$

$$u_d \frac{du_d}{d\xi} = \frac{\tilde{n}_{d0}(1 - P_0\tilde{\phi}_{d0})}{P_0}\left(-Z_d\frac{d\eta}{d\xi} + f_g + f_i\right), \tag{21}$$

$$\frac{d\tilde{n}_d}{d\xi} = -\frac{\tilde{n}_d}{u_d^2}\frac{\tilde{n}_{d0}(1 - P_0\tilde{\phi}_{d0})}{P_0}\left(-Z_d\frac{d\eta}{d\xi} + f_g + f_i\right), \tag{22}$$

$$\frac{d^2\eta}{d\xi^2} = \delta^2\tilde{n} - e^{-\eta} - (\delta^2 - 1 - \delta^2\tilde{\phi}_d P_0)e^{-\eta/\beta} - Z_d\tilde{n}_d, \tag{23}$$

where f is the normalized force as

$$f_g = \frac{F_g \lambda_D}{kT_L}, \qquad f_i = \frac{F_i \lambda_D}{kT_L}, \tag{24}$$

and the subscript 0 denotes the quantities evaluated at the sheath edge. Integrating Eqs. (19) - (23) with the initial values at $\xi = 0$, we obtain $\tilde{n}, \tilde{n}_L, \tilde{n}_H, u, u_d, \tilde{n}_d, Z_d, f_i$, and η as functions of ξ. At the sheath edge, we assume that the potential and the electric field are approximately zero ($\eta \simeq 0$, $d\eta/d\xi \simeq 0$). We should note that the control parameters in the model equations are P_0, δ^2, β, δ_{in}, γ, and q. The values of a, T_L, and $\tilde{n}_{d0}$ determine P_0, and Fig. 1 provides $\tilde{\phi}_{d0}$ (and Z_{d0}). From the definition of P_0 and from the quasi-neutrality condition, the initial value of $\tilde{n}_d$ is $\tilde{n}_{d0} = \delta^2 \tilde{\phi}_{d0} P_0 / Z_{d0}$. The initial values of u and u_d at the sheath edge should be chosen. We should note that this study assumes that the low-temperature electrons are the majority and that the high-temperature electrons are the minority (note the variation range of δ^2) [30]. Thus, the effect of hot electrons on the enhancement of the ion density via ionization (*i.e.*, the dependence of q on δ^2) can be neglected.

III. ION VELOCITY AT THE SHEATH EDGE

Poisson's equation, Eq. (23), can be integrated once by multiplying both sides by $d\eta/d\xi$; then, we obtain

$$\frac{1}{2}\left(\frac{d\eta}{d\xi}\right)^2 + V(\eta) = \frac{1}{2}\left(\frac{d\eta}{d\xi}\bigg|_{\xi=0}\right)^2, \tag{25}$$

where $(d\eta/d\xi|_{\xi=0})^2 \approx 0$ is the weak presheath electric field, and the Sagdeev potential is

$$V(\eta) = \int_0^\eta \big[e^{-\eta} + (\delta^2 - 1 - \delta^2 \tilde{\phi}_d P_0) e^{-\eta/\beta} + Z_d \tilde{n}_d - \delta^2 \tilde{n}\big] d\eta. \tag{26}$$

Thus, based on the monotonic potential drop across the sheath, we can write

$$\frac{d^2 V(\eta)}{d\eta^2}\bigg|_{\eta=0} = \left(\frac{\partial \tilde{n}_L}{\partial \eta} + \frac{\partial \tilde{n}_H}{\partial \eta} + \frac{\partial}{\partial \eta}(Z_d \tilde{n}_d) - \delta^2 \frac{\partial \tilde{n}}{\partial \eta}\right)\bigg|_{\eta=0}, \tag{27}$$

where $\tilde{n}_L = e^{-\eta}$ and $\tilde{n}_H = (\delta^2 - 1 - \delta^2 \tilde{\phi}_d P_0) e^{-\eta/\beta}$. For collisionless, continuous, and cold ions, Eqs. (19) and (20) are reduced to

$$\frac{d}{d\xi}(\tilde{n} u) = 0, \quad (u - \frac{1}{u\gamma})\frac{du}{d\xi} = \frac{d\eta}{d\xi}. \tag{28}$$

Using this,

$$\frac{\partial \tilde{n}}{\partial \eta}\bigg|_{\eta=0} = \frac{\partial \tilde{n}}{\partial \xi} \Big/ \frac{\partial \eta}{\partial \xi}\bigg|_{\eta=0} = -\frac{1}{u_0^2 - 1/\gamma}. \tag{29}$$

Note that

$$\frac{\partial \tilde{n}_L}{\partial \eta}\bigg|_{\eta=0} = -1, \quad \frac{\partial \tilde{n}_H}{\partial \eta}\bigg|_{\eta=0} = -\frac{1}{\beta}(\delta^2 - 1 - \delta^2 \tilde{\phi}_{d0} P_0) \tag{30}$$

If we neglect the ion drag and the gravitational force, Eq. (14) (and Eq. (21)) becomes

$$u_d \frac{du_d}{d\xi} = -\tilde{\phi}_d \frac{d\eta}{d\xi}. \tag{31}$$

Integrating from $\eta = 0$ to η and setting $\Psi = -\int_0^\eta \tilde{\phi}_d \, d\eta$, we can get the dimensionless dust density by utilizing Eq. (17):

$$\tilde{n}_d = \frac{\tilde{n}_{d0}}{\sqrt{1 + 2\Psi/u_{d0}^2}}. \tag{32}$$

If we assume that Z_d does not vary much with η at the sheath edge, we have

$$\begin{aligned} \frac{\partial}{\partial \eta}(Z_d \tilde{n}_d)\bigg|_{\eta=0} &= Z_{d0} \tilde{n}_{d0} \frac{\partial}{\partial \eta}\left(\frac{1}{\sqrt{1 + 2\Psi/u_{d0}^2}}\right)\bigg|_{\eta=0} \\ &= \frac{Z_{d0} \tilde{n}_{d0} \tilde{\phi}_{d0}}{u_{d0}^2}. \end{aligned} \tag{33}$$

Analogous to the analysis of a particle in a potential well, the potential $V(\eta, u_0, u_{d0}) < 0$ in the sheath, which leads to

$$\begin{aligned} \frac{d^2 V(\eta)}{d\eta^2}\bigg|_{\eta=0} &= -1 - \frac{1}{\beta}(\delta^2 - 1 - \delta^2 \tilde{\phi}_{d0} P_0) + \frac{\delta^2 \tilde{\phi}_{d0}^2 P_0}{u_{d0}^2} \\ &\quad + \frac{\delta^2}{u_0^2 - \frac{1}{\gamma}} \le 0. \end{aligned} \tag{34}$$

Therefore, a modified Bohm criterion can be written as

$$u_0^2 \ge \frac{1}{\gamma} + \frac{\delta^2}{1 + \frac{\delta^2 - 1 - \delta^2 \tilde{\phi}_{d0} P_0}{\beta} - \frac{\delta^2 \tilde{\phi}_{d0}^2 P_0}{u_{d0}^2}}. \tag{35}$$

An analysis of a particle in the Sagdeev potential provides relations between δ^2, β, P_0, u_0, and u_{d0}. The ion critical Mach number u_{0crit} depends on P_0, δ^2, β, γ, and u_{d0}, as well as the dust charge at z =0. Figure 2(a) indicates that the velocity of ions entering the sheath must exceed the ion sound velocity because of the dust electrostatic drag force which is in the $-z$ direction [23]. For small P_0, the ion critical Mach number increases with increasing P_0. A further increase in P_0 to a certain level, however, leads to a depletion of the electrons and a consequent reduction in the dust surface potential (dust charge), which makes the dust electrostatic drag force small. Therefore, the ion critical Mach number begins to decrease. Liu *et al.* [23] numerically showed that the ion drift speed into the sheath reaches a maximum and decreases afterward with increasing dust density. Also, the larger δ^2, the larger the ion Mach number is because if the ion density relative to the hot

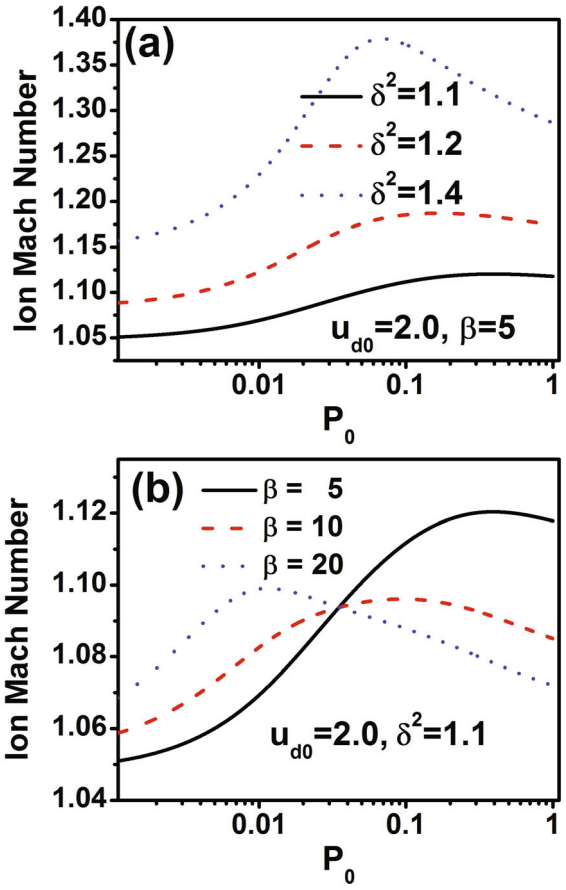

Fig. 2. (Color online) (a) Ion critical Mach number versus P_0 for different δ^2 (= 1.1, 1.2, 1.4). (b) Ion critical Mach number versus P_0 for different β (= 5, 10, 20).

electrons becomes smaller, then the ion should have a larger speed to achieve the formation of a stable sheath.

Figure 2(b) illustrates how the behavior of the ion Mach number vs P_0 curves are modified by the temperature ratio of hot to cold electrons (β (= 5, 10, and 20)). In the discharges with higher values of β , the critical ion speed increases first with increasing P_0, has a maximum and then decreases. The P_0 at the maximum critical ion Mach number shifts to a larger value with decreasing β. The plasma evolution is caused by a collection of background electrons and ions near the electrode (wall) and the dust particles. In the higher β region where hot electrons have higher thermal motions, the dust grain density that causes the critical ion Mach number to be maximum becomes lower.

IV. RESULTS AND DISCUSSION

The main focus of this paper is placed on the investigation of the effects of the population ratio of hot electrons and of the temperature ratio of hot to cold electrons on the sheath properties, which include the spatial distributions of the electric potential, the velocities and the densities of ions and electrons (hot and cold), the velocity and density of dust particles, the dust charge number, the electric force, and the ion drag force along the sheath toward the negatively-biased planar wall. In dusty plasmas, those effects may also depend on the Havnes parameter.

The spatial distributions of η, u, $\tilde{n}$, $\tilde{n}_L$, $\tilde{n}_H$, u_d, $\tilde{n}_d$, Z_d, $Z_d\frac{d\eta}{d\xi}$, and f_i are calculated for different δ^2, β, and P_0. For that purpose, Eqs. (19)-(23) are solved numerically by using the fourth-order Runge-Kutta method with initial conditions. We have chosen the parameter $n_0 = 1.5 \times 10^{10}$ cm^{-3}, $T_L = 2$ eV, $a = 6$ μm, $\rho_d = 2$ g/cm^3, $u_0 = 1.2$, and $u_{d0} = 2$.

First, we study the effects of the population ratio of hot electrons on the sheath structure. Figures 3(a) and 3(b) show the profiles of the normalized electric potential and ion velocity for three different δ^2 (= 1.1, 1.2, and 1.4). Here, $\gamma = 50$, $P_0 = 0.00001$, $q = 0.001$, $\beta = 5$, and $\delta_{in} + \delta_{id} = 3.0$ are used. With an increase in δ^2 ($\delta^2 - 1$ is the density ratio of hot to cold electrons), the electric potential decreases slowly (monotonically), and the sheath width increases. Because more electrons can easily overcome the decelerating electric field force, more charged particles are needed to shield the electric field of the electrode. Consequently, the resulting electric field can be seen to decrease with increasing δ^2. After entering the sheath, due to the effect of the electric field, the ions accelerate slowly for the larger δ^2 case. Hence, far from the plasma - sheath boundary, the ions become faster in a lower δ^2 discharge.

Figure 3(c) illustrates the profiles of the normalized densities of ions ($\tilde{n}$) and electrons ($n_e/n_{e0} = (n_{eL} + n_{eH})/(n_{eL0} + n_{eH0})$) along the distance for different δ^2. From the ion continuity equations, the ion density is inversely proportional to the ion velocity, thus the ion density decreases towards the wall, as the ion velocity increases. The densities of ions and electrons are observed to decrease slowly toward the wall with increasing δ^2.

Figures 3(d) − (f) present the spatial profiles of the normalized velocity, number density, and charge number of the dust particles. We note that away from the sheath edge, the electric force, the gravitational force, and the ion drag force balance, so the total force becomes zero. At this point, the dust velocity and its number density reach a local minimum and maximum, respectively [15]. The charge reversal point corresponds to the position of the maximum dust number density. The position of the charge reversal point is closely related to the curvature of the modeled potential, which is proportional to the electric field at the sheath edge, $E_s = kT_e/e\lambda_i$ (λ_i being the ion collision mean free path) [18]. As δ^2 is increased, the dust velocity increases, and the dust density decreases. This is mainly due to the decrease in the electric field in the sheath. With increasing δ^2, the charge reversal point shifts slightly towards the wall and the maximum

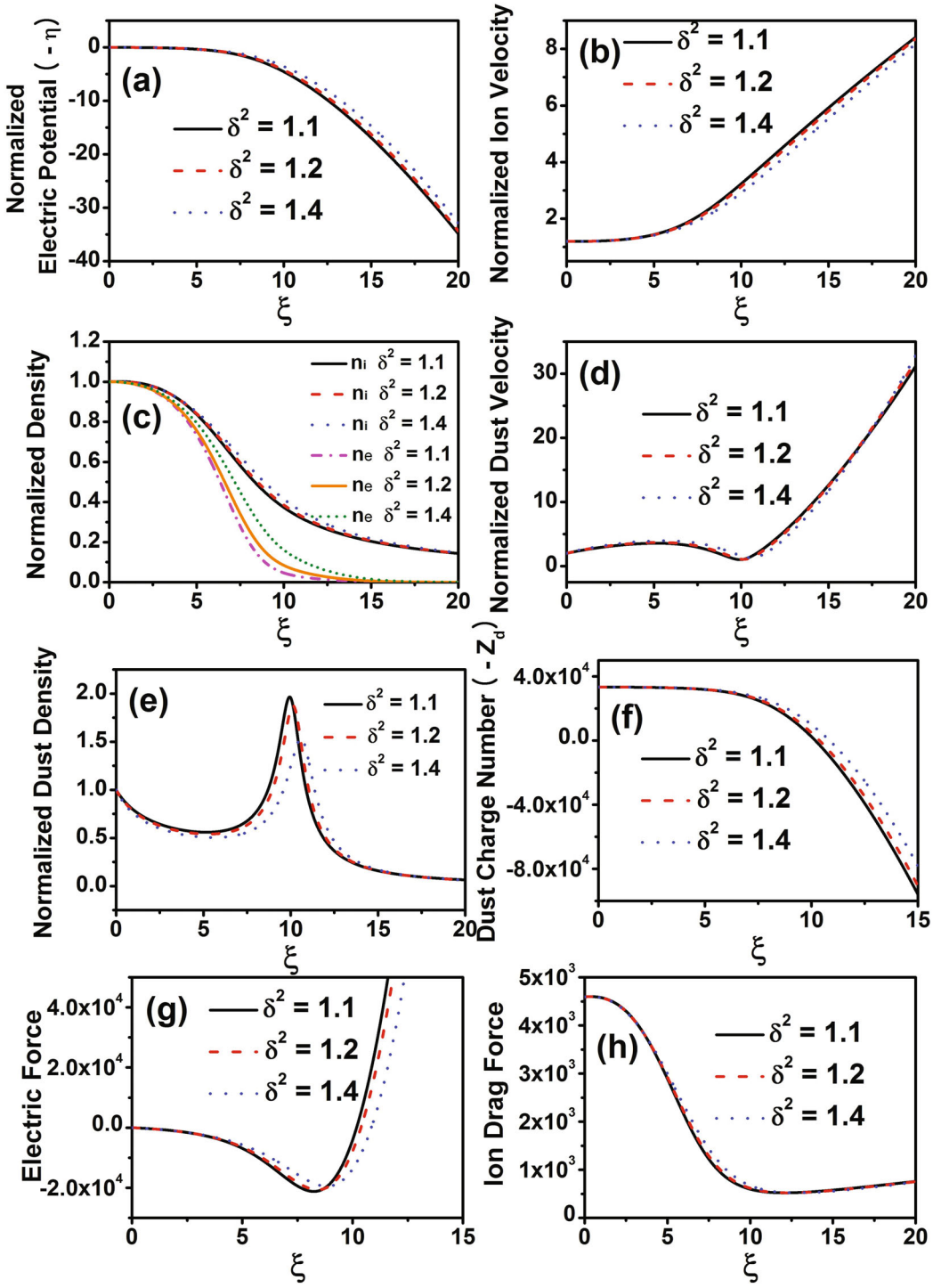

Fig. 3. (Color online) (a) Normalized potential (η), (b) normalized ion velocity (u), (c) normalized densities of ions and electrons ($\tilde{n}$ and n_e/n_{e0}), (d) normalized dust velocity (u_d), (e) normalized dust density (n_d/n_{d0}), (f) dust charge number ($-Z_d$), (g) electric force ($-Z_d \frac{d\eta}{d\xi}$), and (h) ion drag force (f_i) along the normalized distance for three different δ^2 (= 1.1, 1.2, 1.4). Here, $\gamma = 50$, $P_0 = 0.00001$, $q = 0.001$, $\beta = 5$, and $\delta_{in} + \delta_{id} = 3.0$ are used.

of the trapped dust particle density becomes less sharp. In other words, an enhanced population of hot electrons causes the trapped dust distribution to be less sharply peaked and the degree of dust grain trapping to be decreased. We note from Fig. 3(f) that the dust charge is negative almost throughout the sheath and that its abso-

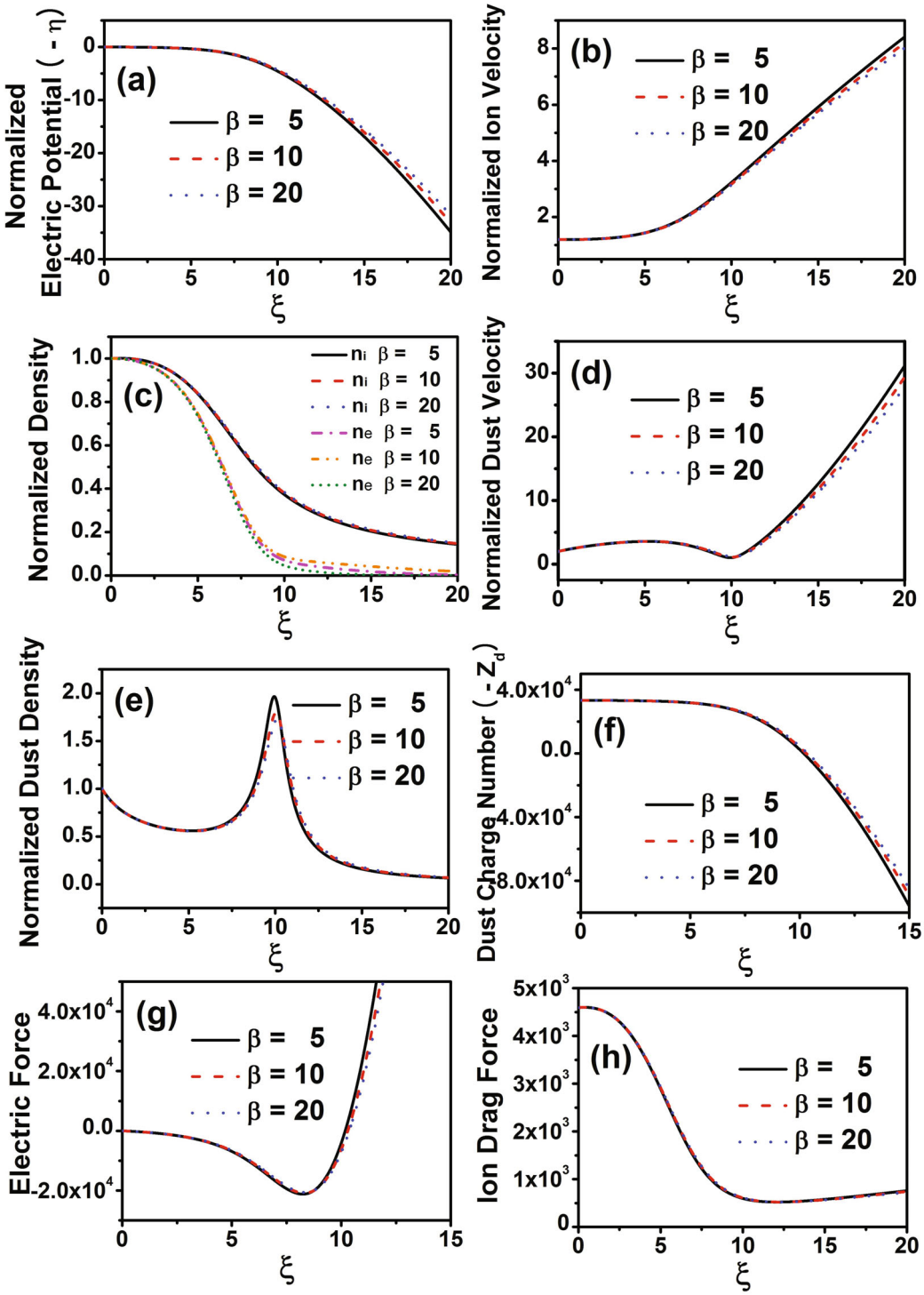

Fig. 4. (Color online) (a) Normalized potential (η), (b) normalized ion velocity (u), (c) normalized densities of ions and electrons ($\tilde{n}$ and n_e/n_{e0}), (d) normalized dust velocity (u_d), (e) normalized dust density (n_d/n_{d0}), (f) dust charge number ($-Z_d$), (g) electric force ($-Z_d\frac{d\eta}{d\xi}$), and (h) ion drag force (f_i) along the normalized distance for different β (= 5, 10, 20). Here, $\gamma = 50$, $P_0 = 0.00001$, $q = 0.001$, $\delta^2 = 1.1$ and $\delta_{in} + \delta_{id} = 3.0$ are used.

lute value decreases from the sheath edge until it changes sign abruptly somewhere close to the wall and then becomes positive. This is due to the fact that the density of electrons falls faster than that of ions in the sheath. Then, the dust grain charge is due only to the ion flux, where the electrons vanish and there is a pure ion sheath

near the wall [24]. As δ^2 is increased, the rate of decrease of the dust charge number becomes small. This can be explained by the contribution of the hot electrons entering the dust grains.

The electric force and the ion drag force corresponding for three different δ^2 are shown in Figs. 3(g) and (h). As δ^2 increases, the electric force is observed to become lower while the ion drag force is observed to become slightly higher. This can be attributed to the fact that the higher δ^2 discharge results in a lower electric field strength (lower slope of the normalized potential shown in Fig. 3(a)) and a slow depletion of the ion density in the sheath (as shown in Fig. 3(c)). As is obvious from Fig. 3(g), the electric force decelerates the dust particles along the sheath before they reach the charge reversal point and then accelerates them. On the other hand, the strength of the electric field increases with increasing distance from the sheath edge. Therefore, the decelerating electric force increases with increasing distance and shows a minimum (the largest negative value) before the charge reversal point [15]. However, the ion drag force always accelerates the dust grains, and its value decreases from the sheath edge due to the decreased ion density and then increases again close to the wall because of the large ion velocity. At the charge reversal point, the electric force vanishes while the ion drag force reaches a minimum.

Next, we investigate the effects of the temperature ratio of hot to cold electrons on the sheath structure. Figures 4(a) and (b) present the normalized electric potential and ion velocity along the distance from the plasma ($\xi = 0$) to the wall for three different β (= 5, 10, and 20). Here, $\gamma = 50$, $P_0 = 0.00001$, $q = 0.001$, $\delta^2 = 1.1$, and $\delta_{in} + \delta_{id} = 3.0$ are used. In the large-β discharges, the hot electrons can easily overcome the decelerating electric field force and hit the wall. Due to the decreasing density of charged particles inside the sheath, a larger volume of charge particles is required to shield the electric field of the electrode. Therefore, the hot electrons and the cold electrons are rarefied slowly along the distance from the bulk plasma sheath edge. As a result, the sheath width broadens, and the electric field decreases with increasing β. The rate of increase of the ion velocity becomes lower due to the decreasing electric field for the larger β case.

Figure 4(c) illustrates the normalized densities of ions and electrons along the distance for different β. The electron density is observed to fall slowly toward the wall, and the sheath width is observed to increase as β is increased. However, the falling profile of the ion density along the sheath depends on β very weakly. In Figs. 4(d) – (f), we have examined the normalized velocity and density of the dust particles, and the dust charge number. As β is increased, the dust velocity increases slightly, and the dust density decreases. This is mainly due to the decrease in the electric field in the sheath. With increasing β, the charge reversal point shifts slightly towards the wall and the maximum of the

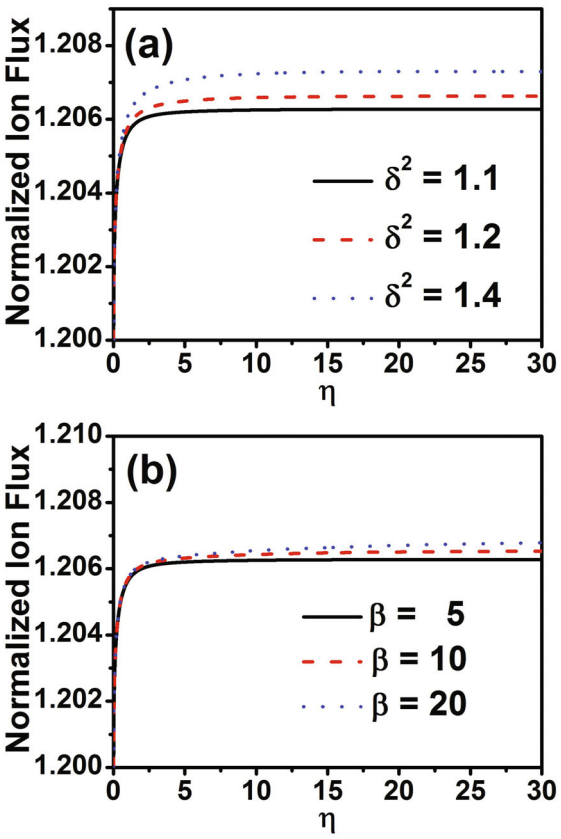

Fig. 5. (Color online) Normalized ion flux entering the probe versus normalized potential for different values of (a) δ^2 and (b) β.

trapped dust particle density becomes less sharp. In other words, an enhanced temperature ratio of hot to cold electrons causes the trapped dust distribution to be less sharply peaked and the degree of dust grain trapping to be decreased. As β is increased, the rate of decrease of the dust charge number becomes small. This can be explained by the contribution of the hot electrons entering the dust grains. The electric force and the ion drag force corresponding to three different β's are shown in Figs. 4(g) and (h). We can note that the magnitude of the electric force decreases slightly with increasing β because the dust charge becomes lower.

If the wall is replaced by a Langmuir probe, a point on the curve of the electric potential at the probe position, $\xi = \xi_p$, gives the normalized potential η_p. The model provides the probe characteristics of the dimensionless ion flux (current) - normalized voltage by plotting $\tilde{n}_{\xi_p} u_{\xi_p}$ versus the dimensionless electric potential η_p. Figures 5(a) – (b) are theoretical $I - V$ curves plotted in this way. Here, we have examined the dependence of the ion flux on δ^2 and β. Clearly, the ion flux increases with both increasing δ^2 and β. With increasing δ^2 and β, the ions should travel further along the sheath to reach a specific electric potential or velocity (as shown in Figs. 3(a) – (b) and 4(a) – (b)). At those distances, the ion

densities under the discharges with higher δ^2 and β are larger than those under the discharges with lower δ^2 and β. The increase in the calculated ion flux originates from the slow depletion of the ion density along the sheath with increasing δ^2 and β, as shown in Figs. 3(c) and 4(c). For dense dusty plasmas with higher P_0 values, the effects of the two-temperature electron distribution on the sheath structure and the ion flux to the probe are found to be not significant. This point can be inferred from the weak dependence of the dust surface potential on both δ^2 and β in the higher P_0 region, as shown in Figs. 1(a) and (b).

V. CONCLUSION

One-dimensional fluid simulations are used to describe a sheath in dusty plasmas with two-temperature electron distributions. The spatial distributions of the electric potential and of the velocities and the densities of the plasma species are calculated in front of a negatively-biased planar wall. The behavior of the dust charge number, the electric force, the ion drag force, and the ion flux collected by the wall are also investigated as functions of the control parameters. The effects of the population ratio of hot to cold electrons and the temperature ratio of hot to cold electrons on the sheath structure are investigated. Based on the Sagdeev potential approach, a modified sheath criterion is obtained theoretically by considering the effect of the two-temperature electrons. Our results show that the high-temperature electrons affect not only the velocity of the ions entering the sheath but also the sheath structure and the ion flux to the wall. We have found that with the increasing temperature or concentration of high-temperature electron, the sheath width increases, the ion flux to the wall is enhanced, and the trapped dust distribution is less sharply peaked. Our results are of direct interest for the control and the probe diagnostics of dust grains in various dusty plasmas with two-temperature electron distributions.

ACKNOWLEDGMENTS

Helpful discussions with Prof. Kyu Sun Chung of Hanyang University and with Dr. Suk Ho Hong of the National Fusion Research Institute of Korea are greatly acknowledged. This work was supported by the research fund of Dong-A University.

REFERENCES

[1] C. K. Goertz, Rev. Geophys. **27**, 271 (1989).
[2] D. A. Mendis and M. Rosenberg, Annu. Rev. Astron. Astrophys. **32**, 419 (1994).
[3] O. Havnes, U. de Angelis, R. Bingham, C. K. Goertz, G. E. Morfill and V. Tsytovich, J. Atmos. Terr. Phys. **52**, 637 (1990).
[4] G. S. Selwyn, J. Singh and R. S. Bennett, J. Vac. Sources Technol. A **7**, 2758 (1989).
[5] L. Boufendi and A. Bouchoule, Plasma Sources Sci. Technol. **11**, A211 (2002).
[6] G. Federici *et al.*, Nucl. Fusion **41**, 1967 (2001).
[7] J. Winter, Plasma Phys. Control. Fusion **46**, B583 (2004).
[8] A. Barkan, N. D'Angelo and R. L. Merlino, Phys. Rev. Lett. **73**, 3093 (1994).
[9] N. C. Adhikary, H. Bailung, A. R. Pal, J. Chutia and Y. Nakamura, Phys. Plasmas **14**, 103705 (2007).
[10] V. V. Yaroshenko, S. A. Khrapak and G. E. Morfill, Phys. Plasmas **20**, 043703 (2013).
[11] A. Bouchoule and L. Boufendi, Plasma Sources Sci. Technol. **2**, 204 (1993).
[12] A. Bouchoule and L. Boufendi, Plasma Sources Sci. Technol. **3**, 292 (1994).
[13] T. Nitter, Plasma Sources Sci. Technol. **5**, 93 (1996).
[14] J-X. Ma and M. Y. Yu, Plasmas **2**, 1343 (1995).
[15] G. Foroutan, Phys. Plasmas **17**, 123711 (2010).
[16] G. Foroutan and A. Akhoundi, J. Appl. Phys. **112**, 073301 (2012).
[17] G. Foroutan and A. Akhoundi, Phys. Plasmas **19**, 103505 (2012).
[18] E. B. Tomme, B. M. Annaratone and J. E. Allen, Plasma Sources Sci. Technol. **9**, 87 (2000).
[19] D. Wang and X. Wang, J. Appl. Phys. **89**, 3602 (2001).
[20] Y. N. Nejoh, Phys. Plasmas **8**, 3545 (2001).
[21] M. K. Mahanta and K. S. Goswami, Phys. Plasmas **8**, 665 (2001).
[22] V. N. Tsytovich, S. V. Vladimirov and S. Benkadda, Phys. Plasmas **6**, 2972 (1999). it failed.
[23] J-Y. Liu, Z-X. Wang, X. Wang, Q. Zhang, X. Zou and Y. Zhang, Phys. Plasmas **10**, 3507 (2003).
[24] D. Benlemdjaldi, A. Tahraoui, R. Hugon and J. Bougdira, Phys. Plasmas **20**, 043508 (2013).
[25] C. Arnas, M. Mikikian and F. Doveil, Phys. Scr. **T89**, 163 (2001).
[26] C. Arnas, M. Mikikian, G. Bachet and F. Doveil, Phys. Plasmas **7**, 4418 (2000).
[27] Yu. I. Chutov, O. Yu. Kravchenko, A. F. Pshenychnyj, R. D. Smirnov, K. Asano, N. Ohno, S. Takamura and Y. Tomita, Phys. Plasmas **10**, 546 (2003).
[28] P. C. Stangeby, Plasma Phys. Control. Fusion **37**, 1031 (1995).
[29] W. D. Jones, A. Lee, S. M. Gleman and H. J. Doucet, Phys. Rev. Lett. **35**, 1349 (1975).
[30] J. Ou, N. Xiang, C. Gan and J. Yang, Phys. Plasmas **20**, 063502 (2013).
[31] T. H. Chung, Phys. Plasmas **21**, 013701 (2014).
[32] S. A. Khrapak, G. E. Morfill, A. G. Khrapak and L. G. Dyachkov, Phys. Plasmas **13**, 052114 (2006).
[33] R. N. Franklin, Plasma Sources Sci. Technol. **9**, 191 (2000).
[34] T. E. Sheridan, P. Chabert and R. W. Boswell, Plasma Sources Sci. Technol. **8**, 457 (1999).
[35] T. E. Sheridan, J. Phys. D: Appl. Phys. **32**, 1761 (1997).
[36] S. A. Khrapak, A. V. Ivlev, G. E. Morfill and H. M. Thomas, Phys. Rev. E **66**, 046414 (2002).